IOP Publishing | International Atomic Energy Agency Nuclear Fusion

Nucl. Fusion **56** (2016) 066007 (11pp) doi:10.1088/0029-5515/56/6/066007

Electromagnetic particle simulation of the effect of toroidicity on linear mode conversion and absorption of lower hybrid waves

J. Bao[1,2], Z. Lin[2,3], A. Kuley[2] and Z.X. Wang[2]

[1] Fusion Simulation Center, Peking University, Beijing 100871, People's Republic of China
[2] Department of Physics and Astronomy, University of California, Irvine, CA 92697, USA

E-mail: zhihongl@uci.edu

Received 19 July 2015, revised 23 February 2016
Accepted for publication 1 April 2016
Published 11 May 2016

Abstract

Effects of toroidicity on linear mode conversion and absorption of lower hybrid (LH) waves in fusion plasmas have been studied using electromagnetic particle simulation. The simulation confirms that the toroidicity induces an upshift of parallel refractive index when LH waves propagate from the tokamak edge toward the core, which affects the radial position for the mode conversion between slow and fast LH waves. Furthermore, moving LH antenna launch position from low field side toward high field side leads to a larger upshift of the parallel refractive index, which helps the slow LH wave penetration into the tokamak core. The broadening of the poloidal spectrum of the wave-packet due to wave diffraction is also verified in the simulation. Both the upshift and broadening effects of the parallel spectrum of the wave-packet modify the parallel phase velocity and thus the linear absorption of LH waves by electron Landau resonance.

Keywords: lower hybrid wave, particle-in-cell simulation, tokamak

(Some figures may appear in colour only in the online journal)

1. Introduction

Since the high current drive efficiency of lower hybrid (LH) waves was discovered using waves with high phase velocity [1, 2], it has been widely applied in the fusion experiments for auxiliary current drive and for controlling magneto-hydrodynamics (MHD) instabilities [3, 4]. The propagation and current drive efficiency of LH waves in various devices have been studied by many linear and quasi-linear theories and simulations, such as Wentzel–Kramers–Brillouin (WKB) and full-wave codes [5–8]. For example, the phase velocity of the injected LH waves is much higher than the phase velocity required for electron Landau damping in many experiments, which is the well-known 'spectral gap' problem. Several mechanisms have been proposed to explain the 'spectral gap' problem from WKB and full-wave simulations, such as toroidicity-induced upshifts of the parallel refractive index [9, 10] and wave scattering and diffractions [6, 11]. However, some experimental phenomena of LH waves are not well understood based on the linear and quasi-linear simulation and theory, such as 'density limit' [12], which is believed to be related to nonlinear processes. For example, parametric decay instabilities of LH waves have been observed in experiments [13–15] and have been studied by some local nonlinear theories [16–19]. In order to understand LH wave nonlinear physics, fully self-consistent and nonlinear kinetic simulation in the realistic toroidal geometry is needed. There are some particle-in-cell codes developed for radio frequency (RF) wave simulations in simple geometry (slab or cylinder), such as GeFi [20–22], Vorpal [23, 24] and G-gauge [25, 26] codes. However, nonlinear simulation of RF waves in the toroidal geometry was not available previously.

[3] Author to whom correspondence should be addressed.

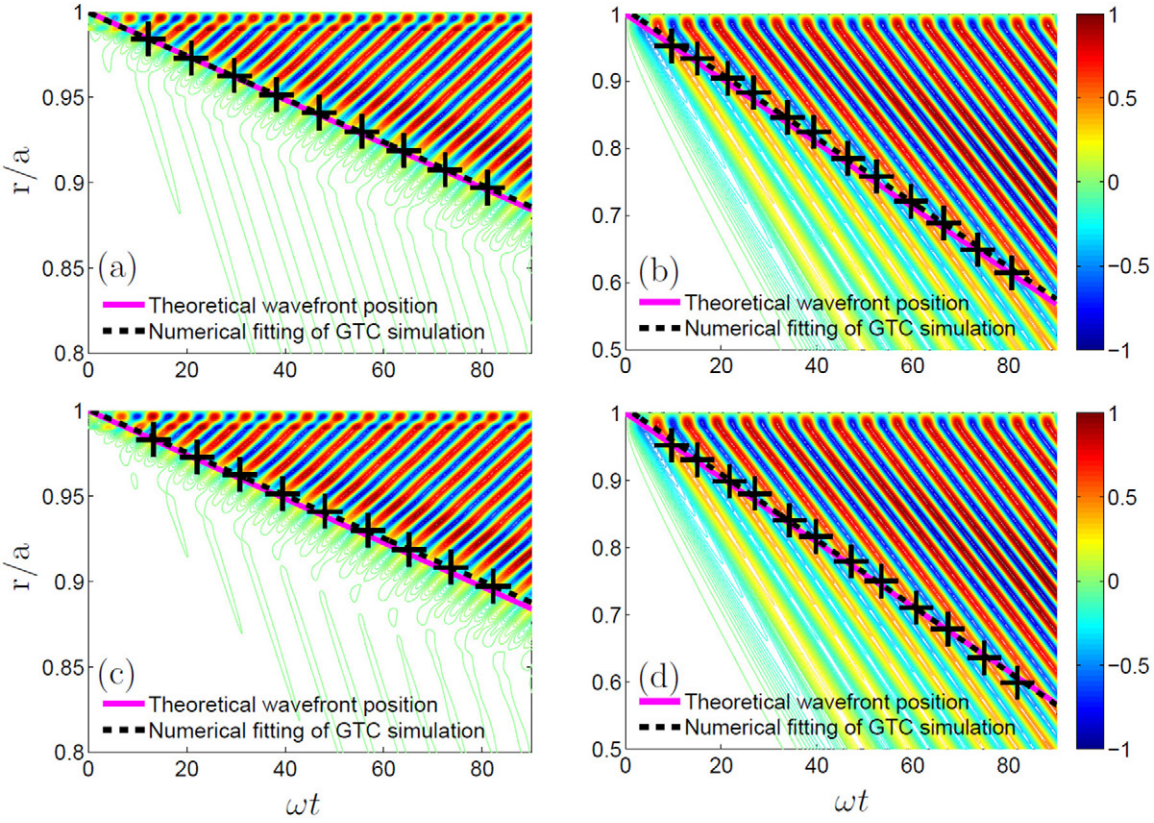

Figure 1. 2D radial-time plots of (*a*) slow LH wave and (*b*) fast LH wave propagations in uniform plasmas from simulations using the electron model with kinetic momentum. 2D radial-time plots of (*c*) slow LH wave and (*d*) fast LH wave from simulations using the electron model with canonical momentum. The purple line is the theoretical wave-front position. The black crosses are the wave-fronts measured from GTC simulation and the black dashed line is the numerical fitting of the wave-fronts. The color scale represents the electrostatic potential ϕ in arbitrary units.

In our recent work [27–31], we have developed nonlinear particle-in-cell (PIC) simulation incorporating the toroidal geometry. Compared to WKB and full-wave approaches for the modeling of LH waves, the PIC approach can address self-consistently the nonlinear dynamics of both the LH wave-packet and particle distribution function. This new capability has been developed using the global gyrokinetic toroidal code (GTC) [32], which has been widely used in studying neo-classical transport [33, 34], microturbulence [35, 36], Alfven eigenmodes [37, 38] and current-driven MHD instabilities [39–41] in tokamak experiments with general magnetic geometry [42]. In an earlier work, GTC simulation of LH wave propagation in the tokamak geometry has been carried out by using a linear electrostatic model [27]. Recently a nonlinear electromagnetic particle model for LH wave simulation has been successfully implemented in GTC, and verified for the LH wave dispersion relation and nonlinear electron trapping [28].

The linear propagation and quasilinear absorption of LH waves in tokamaks have been widely studied by the WKB and full-wave simulations, and several factors have been found to fill the 'spectral gap' [43]. The toroidicity can lead to the upshift of the parallel refractive index $n_{||}$ during the LH wave propagation, which can be modelled with ray-tracing code very well [10, 44]. Meanwhile, the wave diffraction and scattering effects can lead to the broadening of the wave-packet both in real space and spectral space, which result in a broader power absorption by the electrons [6, 11].

In this paper, we apply GTC to simulate the effects of toroidicity on the linear mode conversion and absorption of LH waves. Firstly, the propagations of the slow and fast LH waves are verified in GTC simulation. Both phase and group velocities of slow and fast LH waves agree with theory very well. Secondly, the mode conversions between slow and fast LH waves are verified in our simulation when the accessibility condition is not satisfied. The simulation confirms that the toroidicity induces an upshift of the parallel refractive index ($n_{||}$) when LH waves propagate from the tokamak edge toward the core, which affects the radial position of the mode conversion between slow and fast LH waves. Furthermore, we confirm that moving the launching position from the low field side to the high field side of the tokamak can lead to a larger upshift of $n_{||}$, which can help the slow LH wave penetrate into the tokamak core by avoiding mode conversion when plasma temperature is low with negligible absorption. Thirdly, in the simulation of LH wave linear absorption in hot plasmas, we observe the upshift and broadening effects of the poloidal spectrum of the LH wave-packet due to the poloidal asymmetry of the equilibrium magnetic field and wave diffractions. These effects change the parallel phase velocity and enhance the linear absorptions of LH waves by electron Landau resonance, which are similar to WKB and full wave simulation results and can be considered as candidates to fill the 'spectral gap'.

Table 1. Comparison of the radial group and phase velocities of the slow and fast LH waves between GTC simulation and the theory.

	Fast LH wave		Slow LH wave	
	$v_g(\mathrm{m\,s^{-1}})$	$v_p(\mathrm{m\,s^{-1}})$	$v_g(\mathrm{m\,s^{-1}})$	$v_p(\mathrm{m\,s^{-1}})$
Theory	-1.93×10^7	-3.98×10^7	-5.09×10^6	1.07×10^7
GTC (canonical momentum electron)	-1.98×10^7	-3.80×10^7	-5.05×10^6	1.08×10^7
GTC (kinetic momentum electron)	-1.93×10^7	-3.80×10^7	-5.08×10^6	1.08×10^7

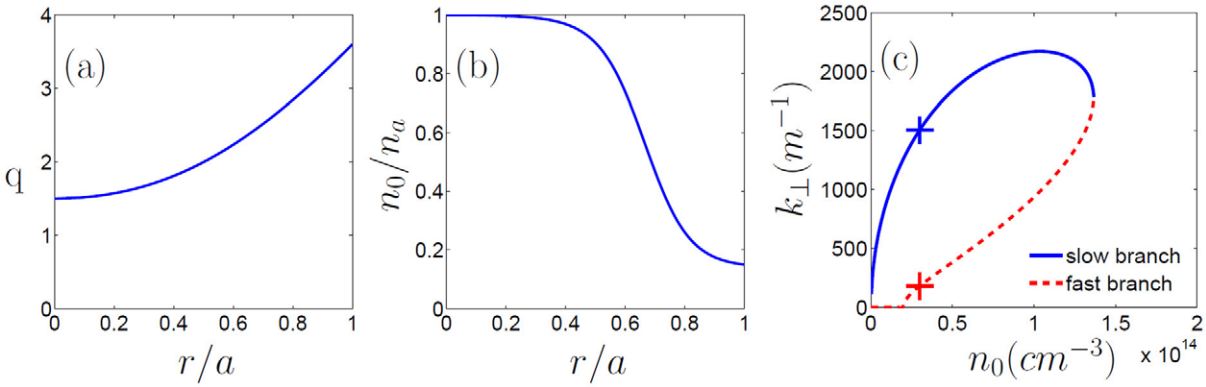

Figure 2. (*a*) The safety factor q and (*b*) the equilibrium density profiles. Panel (*c*) is the dependence of the LH wave's perpendicular wave vector on the plasma density with a fixed $n_{||}$. The blue and red crosses represent the launched perpendicular wave vectors of slow and fast LH waves, respectively.

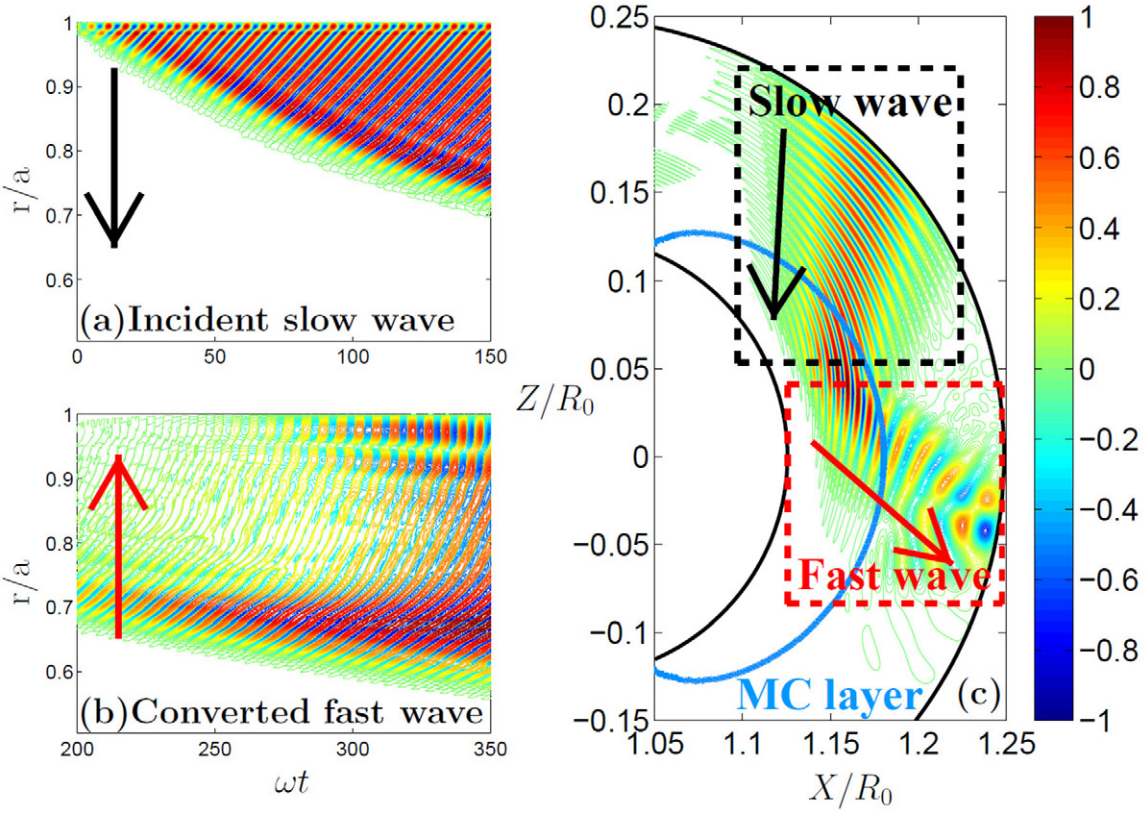

Figure 3. The 2D radial-time plot of (*a*) the incident slow LH wave and (*b*) the mode converted fast LH wave in GTC simulation. Panel (*c*) shows the mode structures of the slow and fast LH waves in the poloidal cross-section. The blue line in (*c*) is the analytic calculation of the mode conversion layer assuming poloidal harmonic $m = 0$. The black and red arrows represent the slow and fast LH wave propagating directions, respectively. The color scale represents the electrostatic potential ϕ in arbitrary units.

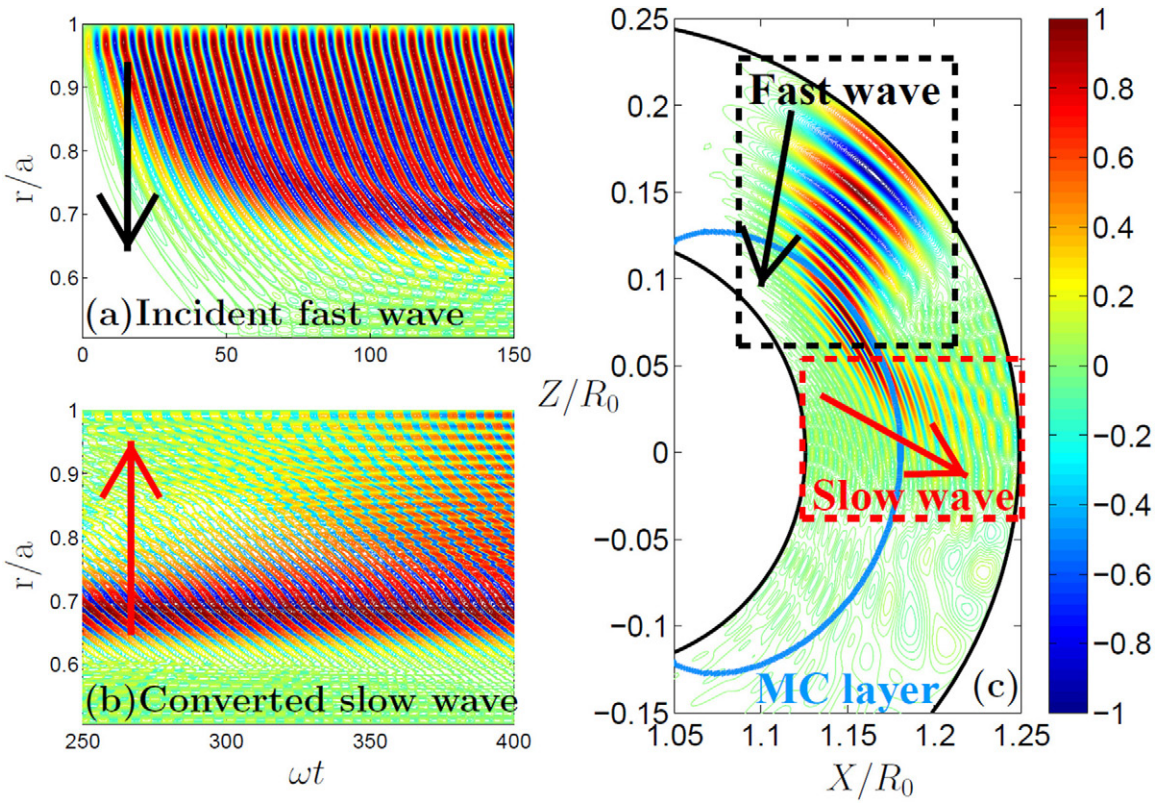

Figure 4. The 2D radial-time plot of (*a*) the incident fast LH wave and (*b*) the mode converted slow LH wave in GTC simulation. Panel (*c*) shows the mode structures of the slow and fast LH waves in the poloidal cross-section. The blue line in (*c*) is the analytic calculation of the mode conversion layer assuming $m = 0$. The black and red arrows represent the fast and slow LH wave propagating directions, respectively. The color scale represents the electrostatic potential ϕ in arbitrary units.

The paper is organized as follows. Linear propagations of the slow and fast LH waves are verified in section 2. Linear mode conversions between slow and fast LH waves in the toroidal geometry are shown in section 3. The LH wave linear absorption in hot plasmas is discussed in section 4. Section 5 gives the conclusion.

2. Verification of slow and fast LH waves' propagation in a cylinder

Recently, we have developed an electromagnetic particle simulation model for LH waves and successfully implemented it into GTC [28], in which ion dynamics is described by a fluid equation and electron dynamics is described by a drift kinetic equation with either kinetic momentum or canonical momentum. The perturbed electron density is calculated by an electron continuity equation, while the perturbed electron velocity is calculated from marker particles. This method can avoid the numerical instability caused by the discrepancy between electron marker distribution and Maxwell distribution for δf simulation. The dispersion relation of slow and fast LH waves and the nonlinear electron trapping have been verified. This model can be applied in studying the linear and nonlinear physics of LH waves.

Using the electromagnetic model, the phase and group velocities of slow and fast LH waves have been verified in uniform cylinder plasmas. In this paper, we apply the following notations: ω_{pe} is electron plasma frequency, ω_{pi} is the ion plasma frequency, Ω_{ce} is the electron cyclotron frequency, Ω_{ci} is the ion cyclotron frequency, ω is the LH wave frequency, $k_{||}$ and $k_{\perp}$ are the parallel and perpendicular wave vectors of LH waves, respectively.

In the simulation, the parallel wave vector of LH wave in a cylinder is $k_{||} = n/R = 100.0\,\mathrm{m}^{-1}$, where $n = 100$ is the parallel mode number, $R = 1.0\,\mathrm{m}$, and the minor radius is $a = 0.3\,\mathrm{m}$. The plasma density $n_{e0} = n_{i0} = 2 \times 10^{13}\,\mathrm{cm}^{-3}$, electron temperature $T_{e0} = 50.0\,\mathrm{eV}$ (for cold plasma approximation with $\omega \gg k_{||}v_{the}$, where $v_{the} = \sqrt{2T_{e0}/m_e}$ is the electron thermal speed) and magnetic field $B = 2.0\,\mathrm{T}$ are uniform, and the magnetic field is only along the axial direction in the cylinder. We have verified the dispersion relation with the same parameters as shown in figure 3 of an earlier work [28]. Using an antenna frequency $\omega/\Omega_{ci} = 70.0$, there are two $k_{\perp}$ values on the LH dispersion relation curve, which correspond to a slow LH wave with $k_{\perp}/k_{||} = 12.58$ and a fast LH wave with $k_{\perp}/k_{||} = 3.37$. Then we use an antenna to launch slow and fast LH waves with the corresponding radial structures ($k_{\perp}$) at the boundary. The 2D radial-time plots of slow and fast LH wave propagations by using both electron models with kinetic momentum and canonical momentum are shown in figure 1. In figures 1(*a*) and (*c*) where the slow LH wave is excited by the antenna, there are very small fast LH wave components which are caused by the numerical coupling between the antenna structure and slow LH wave eigenmode.

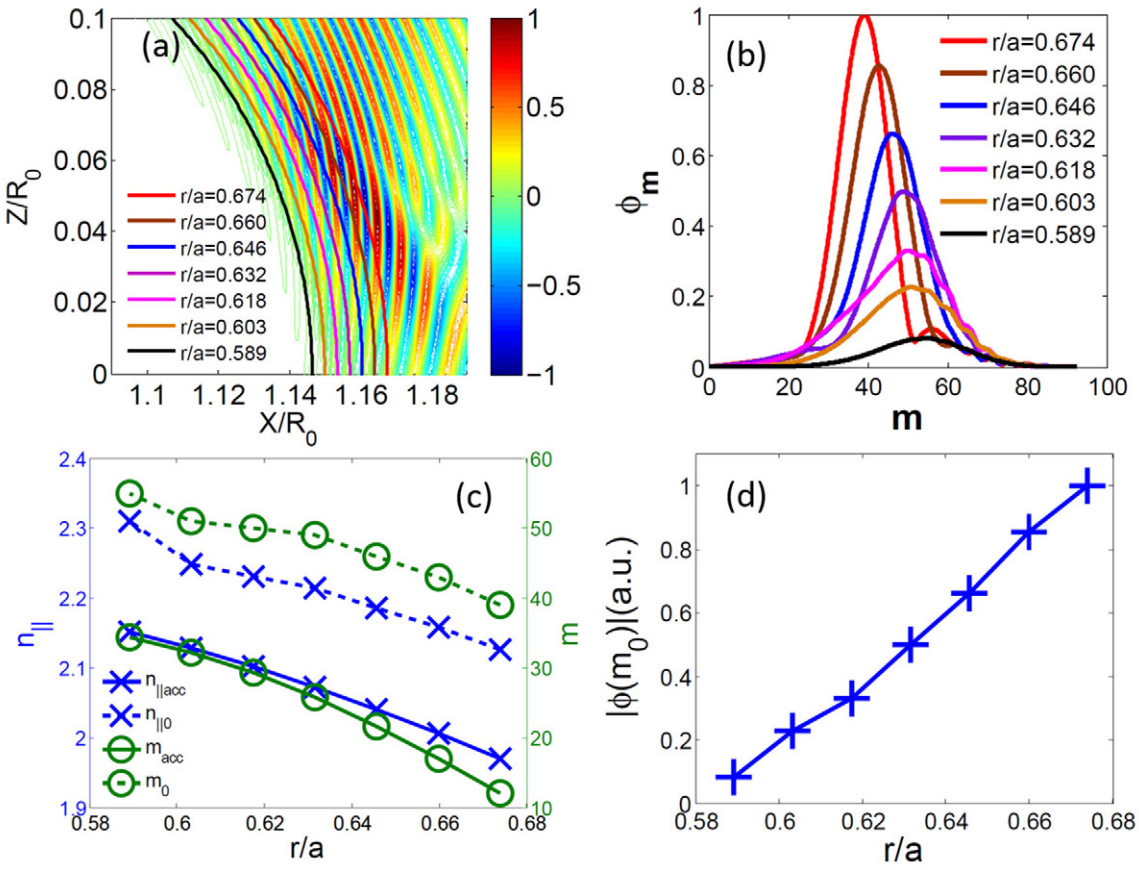

Figure 5. (*a*) The positions of the flux surfaces for poloidal spectrum examination. (*b*) The poloidal m spectrum of the LH wave-packet near the mode conversion region. (*c*) The radial dependence of the central parallel refractive index $n_{||0}$ and poloidal mode number m_0 of the LH wave-packets, and their comparisons with the threshold values of the accessibility condition. Blue and green solid lines are local threshold values of parallel refractive index and poloidal spectrum, respectively. Blue and green dashed lines are the central values of the parallel refractive index and poloidal spectrum of the LH wave-packet, respectively. (*d*) is the amplitude of the central poloidal component of the LH wave-packet at different flux surfaces near the mode conversion region.

There are also very small slow LH wave components in figures 1(*b*) and (*d*), which are similarly caused by the numerical coupling between the antenna structure and fast LH wave eigenmode. Next, we measure the coordinates of the points at half maximum potential value as the wave-fronts in the radial-time space to derive the wave-front line from GTC simulation. In figures 1(*a*)–(*d*), the slope of the wave-front line in the radial-time space provides the radial group velocity (v_g) of the corresponding wave, and the slope of the potential structure with the same phase gives the radial phase velocity (v_p). The comparisons of group and phase velocities of the LH waves between GTC simulations and the analytical theory are given in table 1. The group velocity is in the opposite direction to the phase velocity for the slow LH wave, while the group velocity is in the same direction with phase velocity for the fast LH wave, which agrees with the linear theory [45].

3. Linear mode conversion between slow and fast LH waves in toroidal geometry

In the LH wave frequency range, there are three branches of waves, i.e. slow LH wave, fast LH wave and ion plasma wave. The slow LH wave branch is used to drive the plasma current since it has a larger parallel electric field and can accelerate the fast electrons. Recently, the fast LH wave branch in LH frequency range (also called 'helicon') is proposed and applied for current drive in a tokamak because it can propagate into the plasma core without a density limit, and can avoid the strong damping near the plasma edge [46]. However, when LH waves propagate to the high density core from the low density edge in tokamak, mode conversion between the slow and fast LH waves will occur if the local accessibility condition is not satisfied, namely, if the parallel refractive index of LH wave is smaller than the threshold value: $n_{||} = ck_{||}/\omega < n_a$, where $n_a = \sqrt{S} + \sqrt{-D^2/P}$, $S = 1 + \omega_{pe}^2/\Omega_{ce}^2 - \omega_{pi}^2/\omega^2$, $D = -\omega_{pe}^2/(\omega\Omega_{ce})$ and $P = 1 - \omega_{pe}^2/\omega^2$. On the other hand, if the accessibility condition is satisfied before the LH wave is absorbed, the incident slow LH wave can convert to the ion plasma wave near the resonant layer [5].

In this section, we will study the linear mode conversion between the slow and fast LH waves in tokamak geometry. We launch the slow and fast LH waves at the plasma edge at $\theta = 0.25\pi$, respectively. We choose the simulation parameters based on the Alcator C-Mod tokamak, which include $a = 0.16\,\mathrm{m}$, $R_0 = 0.64\,\mathrm{m}$ and the axis value of the magnetic field $B_a = 5.0\,\mathrm{T}$. The plasma density is non-uniform with

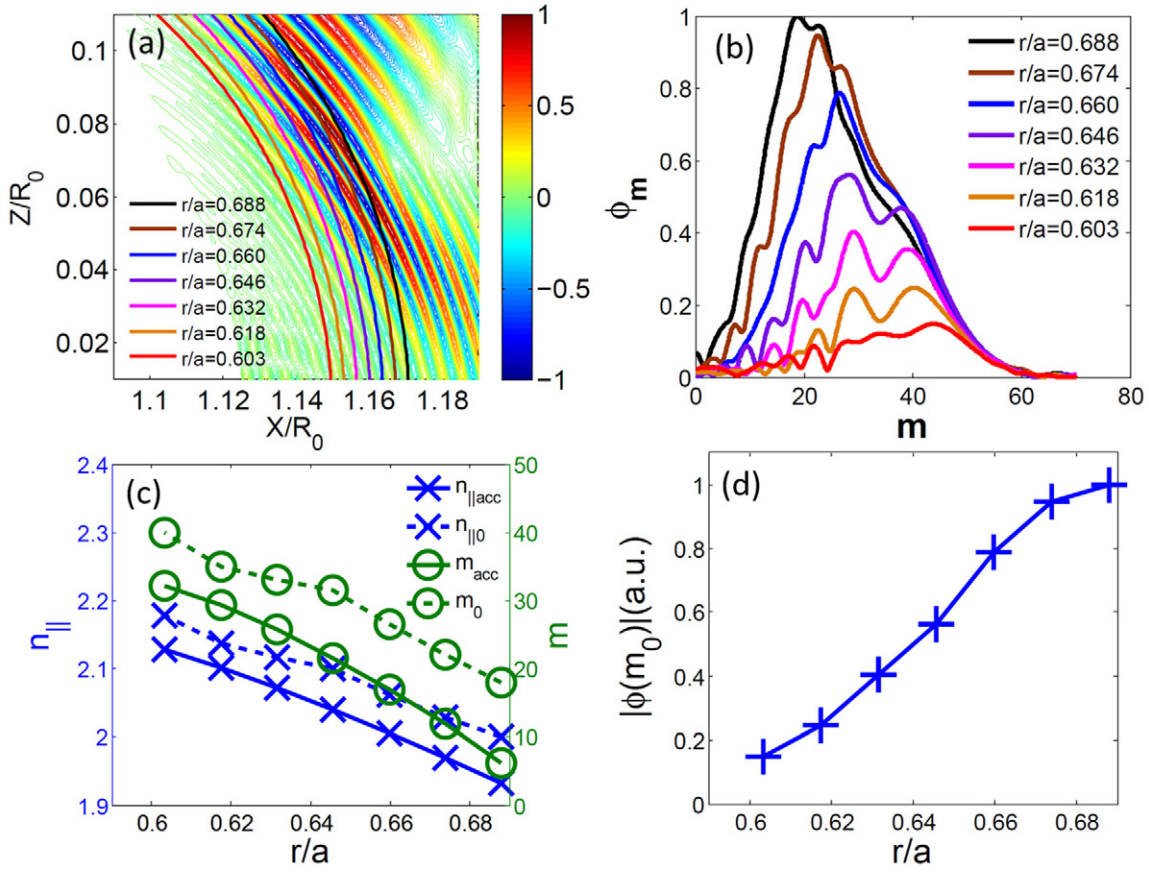

Figure 6. (*a*) The positions of the flux surfaces for poloidal spectrum examination. (*b*) The poloidal m spectrum of the LH wave-packet near the mode conversion region. (*c*) The radial dependence of the central parallel refractive index $n_{||0}$ and poloidal mode number m_0 of the LH wave-packets, and their comparisons with the threshold values of the accessibility condition. Blue and green solid lines are local threshold values of parallel refractive index and poloidal spectrum, respectively. Blue and green dashed lines are the central values of the parallel refractive index and poloidal spectrum of the LH wave-packet, respectively. (*d*) is the amplitude of the central poloidal component of the LH wave-packet at different flux surfaces near the mode conversion region.

axis value $n_{i0} = n_{e0} = 2.0 \times 10^{14}\,\mathrm{cm}^{-3}$, which is closer to the ITER regime [47] and can be operated on the Alcator C-Mod tokamak [48, 49]. An antenna with a Gaussian profile [27] in the poloidal direction is applied with the central poloidal spectrum number $m_0 = 0$ in the plasma edge, which can produce the LH wave fluctuations with the launched frequency $f_0 = 4.6\,\mathrm{GHz}$ and the toroidal refractive index $n_t = ck_t/\omega = 1.86$, where $k_t = n/R$ is the toroidal wave vector. However, the electron temperature is setting as $T_{e0} = 50\,\mathrm{eV}$, which is not true in experiments. This temperature is used firstly for a cold plasma with $\xi_e = \omega/(k_{||}v_{the}) \approx 53.6$ to give negligible wave damping. The safety factor q and the equilibrium density profiles are shown in figures 2(*a*) and (*b*). If the accessibility condition is not satisfied, the mode conversion between slow and fast LH waves will happen as the wave propagates to the high density area as shown in figure 2(*c*). The blue and red crosses in figure 2(*c*) represent the launched perpendicular wave vectors of the slow and fast LH waves, respectively.

When the slow LH wave launched by the antenna propagates toward the tokamak core, we observe that the incident slow LH wave can convert to the fast LH wave as shown in figure 3. Figures 3(*a*) and (*b*) show the structures of the incident slow LH wave and mode converted fast LH wave in radial-time space, respectively. The LH wave pattern structure on the poloidal plane is shown in figure 3(*c*). Similarly we launch the fast LH wave at the same antenna position, the incident fast LH wave can also convert to the slow LH wave as shown in figure 4. Figures 4(*a*) and (*b*) show the structures of the incident fast LH wave and mode converted slow LH wave in radial-time space, respectively. The LH wave pattern structure on the poloidal plane is shown in figure 4(*c*). The mode conversion layer is also calculated by assuming the poloidal harmonic number of the wave-packet $m = 0$, which is shown by the blue lines in figures 3(*c*) and 4(*c*). The difference of the mode conversion layer between simulation and anayltic calculation assuming $m = 0$ is due to the evolution of the m number of the wave-packet during propagation in toroidal geometry. In the toroidal geometry, the relation between $k_{||}$ and m is $k_{||} = (n + m/q)/R$ for the perturbation with the phase: $\exp(\mathrm{i}m\theta + \mathrm{i}n\zeta)$ along poloidal θ and toroidal ζ directions in our simulation, where a single toroidal mode $n = 135$ is launched by the antenna and m number could be negative or positive during the evolution. The positive increase of m number will lead to the increase of the parallel refractive index $n_{||} = ck_{||}/\omega$, which helps to satisfy the accessibility condition. In order to derive the poloidal spectrum of

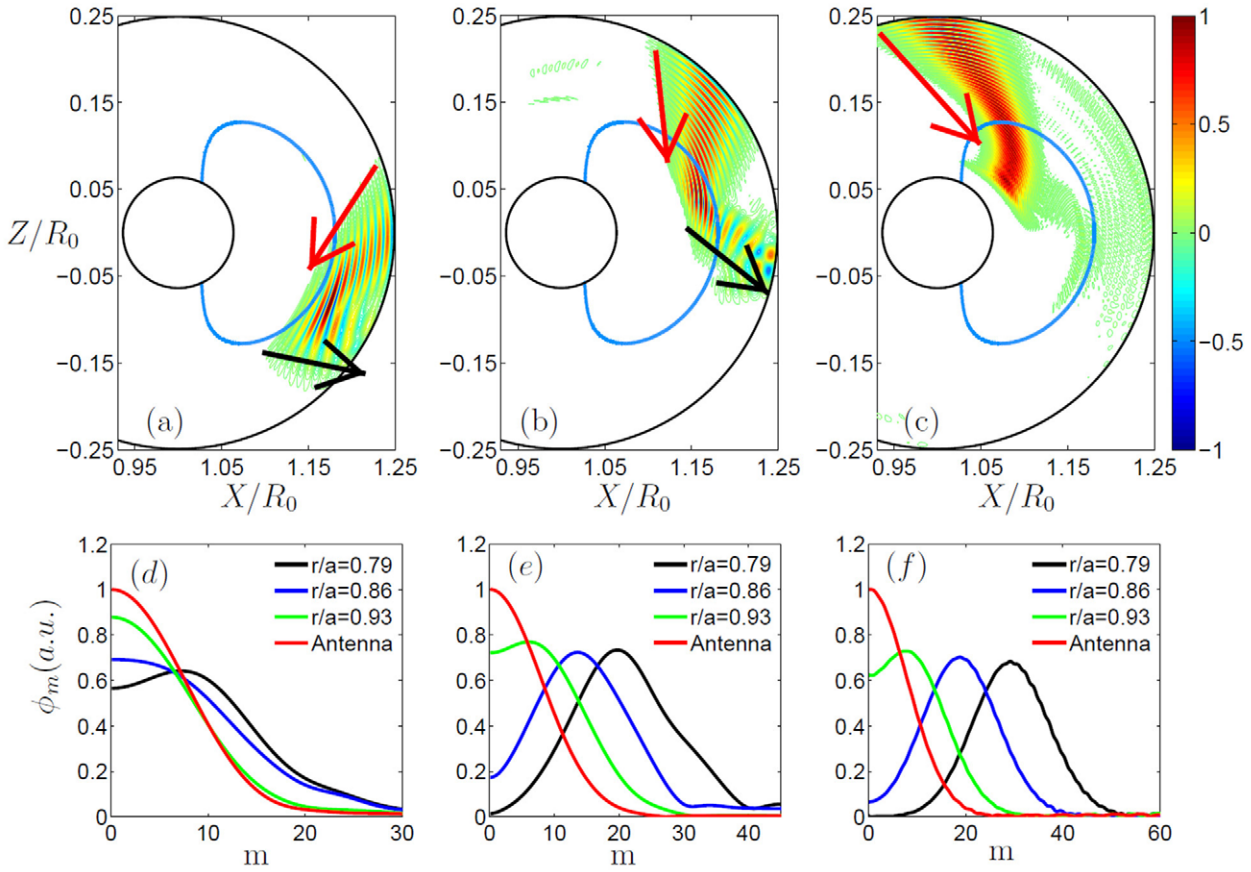

Figure 7. The slow LH wave is launched from poloidal angle (*a*) $\theta = 0$, (*b*) $\theta = 0.25\,\pi$ and (*c*) $\theta = 0.5\,\pi$, respectively. The blue line is the calculation of the mode conversion layer assuming $m = 0$. Panels (*d*)–(*f*) are the corresponding poloidal spectrums of the slow LH wave-packets at different flux-surfaces. The red and black arrows represent the slow and fast LH wave propagating direction, respectively. The color scale represents the electrostatic potential ϕ in arbitrary units.

the LH wave-packet, we choose several flux surfaces near the mode conversion layer to perform the Fourier transform. From the corresponding poloidal spectrum in figures 5(*b*) and 6(*b*), it is observed that the central poloidal mode number m_0 of the LH wave-packet near the mode conversion layer has a larger increase compared to the initial launched wave-packet with $m_0 = 0$, and the low poloidal components of the wave-packet vanish when the wave-packet propagates through the mode conversion layer. During the mode conversion, the central poloidal mode number of the wave-packet increases so that the wave-packet in the inner side of the mode conversion layer can satisfy the accessibility condition. In figures 5(*c*) and 6(*c*), we compare the central parallel refractive index and the poloidal mode number of the wave-packet with the local threshold values of accessibility condition, respectively. It is observed that the survived LH wave-packet (not be reflected) can satisfy the local accessibility condition for both cases of the mode conversion. However, the amplitude of the central poloidal component decreases as the LH wave propagates through the mode conversion layer, as shown in figures 5(*d*) and 6(*d*), which means the energy of the incident wave-packet is gradually taken away by the converted waves. In these two cases of mode conversion, the reflections of the incident slow and fast LH waves at the mode conversion layer are weak since the equilibrium density scale length is much longer than the LH wave length [50, 51].

Launching LH waves from different poloidal angle positions of the tokamak will lead to different propagations and absorptions. For example, recently launching LH waves from the high field side is proposed due to many significant advantages such as the relaxed accessibility condition [52, 53] and the strong poloidal wave number upshift for alpha particle channeling [54, 55]. We now study the LH wave propagation from different launching positions in tokamaks. We launch the slow LH wave at the poloidal angle $\theta = 0$, $\theta = 0.25\pi$ and $\theta = 0.5\pi$, respectively, as shown in figures 7(*a*)–(*c*). The poloidal spectra of the slow LH wave-packets at different flux-surfaces are measured during the mode conversion. We find that moving the launch position from the low field side toward the high field side can lead to a larger increase of the central poloidal number m_0 as shown in figures 7(*d*)–(*f*), namely, a larger increase of the parallel refractive index $n_{||}$, which is helpful for the wave penetration into the core plasma by avoiding the mode conversion. Although a similar conclusion has been derived from WKB simulation [5, 52, 53], it is verified by the particle simulation in toroidal geometry for the first time. Since we want to study here the poloidal spectrum evolution effects on mode conversion, the simulations are carried

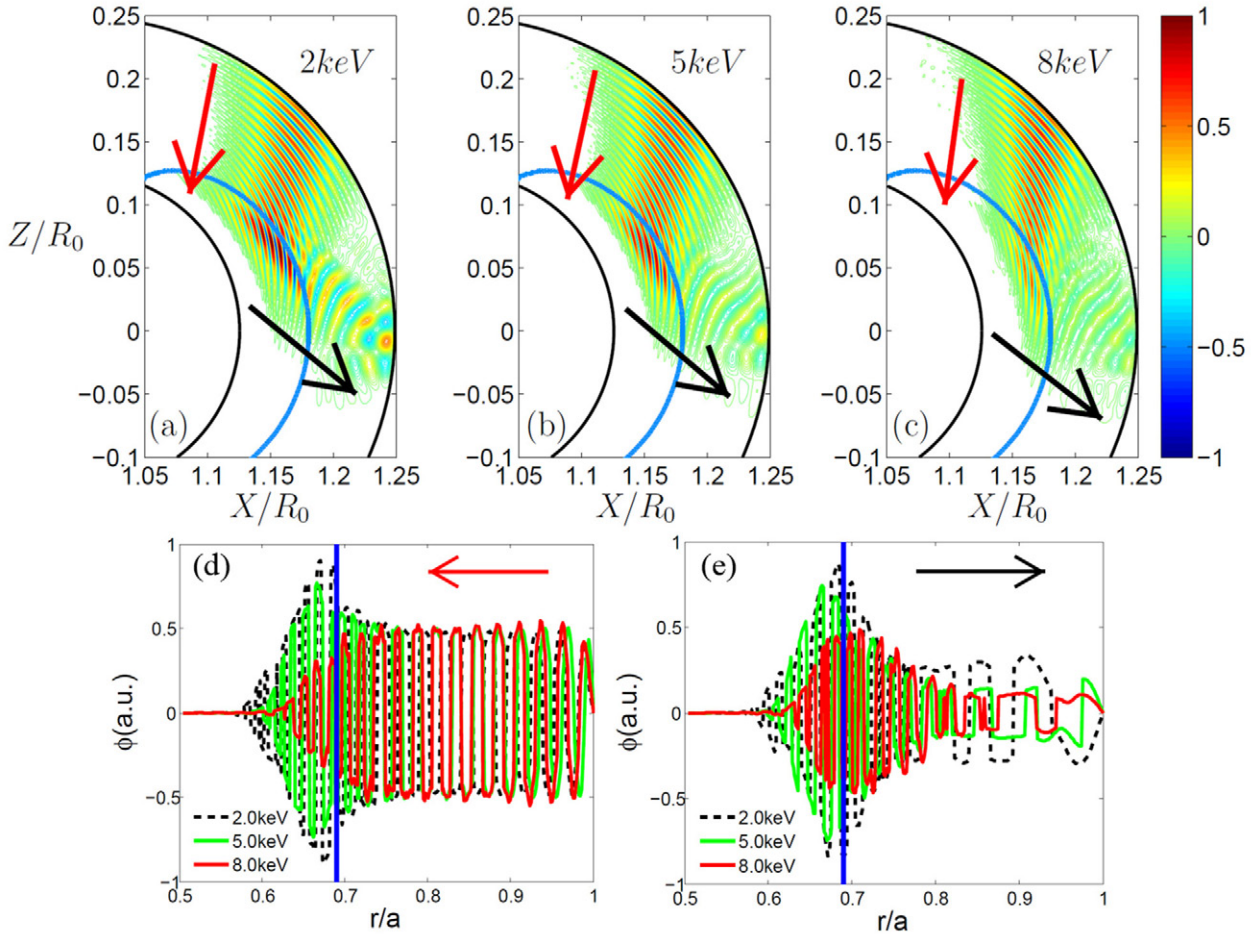

Figure 8. Panels (*a*)–(*c*) are the LH wave structures in poloidal sections with 2.0, 5.0 and 8.0 keV electron temperature, respectively. The color scale represents the electrostatic potential ϕ in arbitrary units. Panels (*d*) and (*e*) are the comparisons of the radial mode structures of the slow and fast LH waves between different electron temperatures, respectively. The red and black arrows represent the radial propagating directions of the slow and fast LH waves, respectively.

out firstly with negligible absorptions (low electron temperature). Mode conversion is the only mechanism to prevent the LH wave from penetrating into the tokamak core. However, it should be pointed out that the larger upshift of the parallel spectrum could induce greater electron Landau damping in hot plasmas.

4. Linear absorption of LH waves in toroidal geometry

In this section, linear absorption of LH waves in the mode conversion and in the single pass propagation in tokamaks is studied in hot plasmas. In the simulation, the axis value of the magnetic field is $B_a = 5.0\,\mathrm{T}$. The minor and major radii of the tokamak are $a = 0.16\,\mathrm{m}$, $R_0 = 0.64\,\mathrm{m}$, respectively. The launched LH wave frequency $f_0 = 4.6\,\mathrm{GHz}$ and the toroidal refractive index $n_t = ck_t/\omega = 1.86$. The plasma temperature is on the order of keV and the plasma density changes from the orders of $10^{13}\,\mathrm{cm}^{-3}$–$10^{14}\,\mathrm{cm}^{-3}$ in different simulation cases. In this regime, the ion perpendicular absorption is much weaker than electron parallel absorption. We have $\xi_e \approx 6.5$ for $T_{e0} = 2.0\,\mathrm{keV}$, $\xi_e \approx 4.1$ for $T_{e0} = 5.0\,\mathrm{keV}$ and $\xi_e \approx 3.3$ for $T_{e0} = 8.0\,\mathrm{keV}$, and $\xi_i \gg \xi_e$ for all cases, where $\xi_i = \omega/(k_\perp v_{thi})$, $v_{thi} = \sqrt{2T_{i0}/m_i}$, and $\xi_e = \omega/(k_{||}v_{the})$ are calculated by using the parameters at the launching position $r/a = 1$. In these regimes, the parallel electron Landau damping is the main absorption mechanism of LH waves. Thus, the fluid ion and drift kinetic electron model is applied in the simulation neglecting the ion absorption.

In the mode conversion cases, the plasma temperature is uniform, while the plasma density is non-uniform with axis value $n_{i0} = n_{e0} = 2.0 \times 10^{14}\,\mathrm{cm}^{-3}$. Figures 8(*a*)–(*c*) show the LH wave pattern structures in the poloidal cross-section with increasing electron temperature from 2.0–8.0 keV. We measure the maximal values of the electrostatic potential at each flux surface for the slow and fast LH wave branches from figures 8(*a*)–(*c*), which give the radial structures of slow and fast LH waves as shown by figures 8(*d*) and (*e*), respectively. It should be pointed out that we use the data between $\theta = \pi/8$ and $\theta = 3\pi/8$ in figures 8(*a*)–(*c*) for the radial structure calculation of slow wave, and use the data between $\theta = 0$ and $\theta = \pi/8$ in figures 8(*a*)–(*c*) for fast wave. In figure 8(*d*), the slow LH wave amplitudes of $T_{e0} = 2.0\,\mathrm{keV}$ and $T_{e0} = 5.0\,\mathrm{keV}$ cases are similar with little damping, while it damps significantly near the mode conversion region for the $T_{e0} = 8.0\,\mathrm{keV}$ case. In figure 8(*d*), the parallel phase velocity of the slow LH

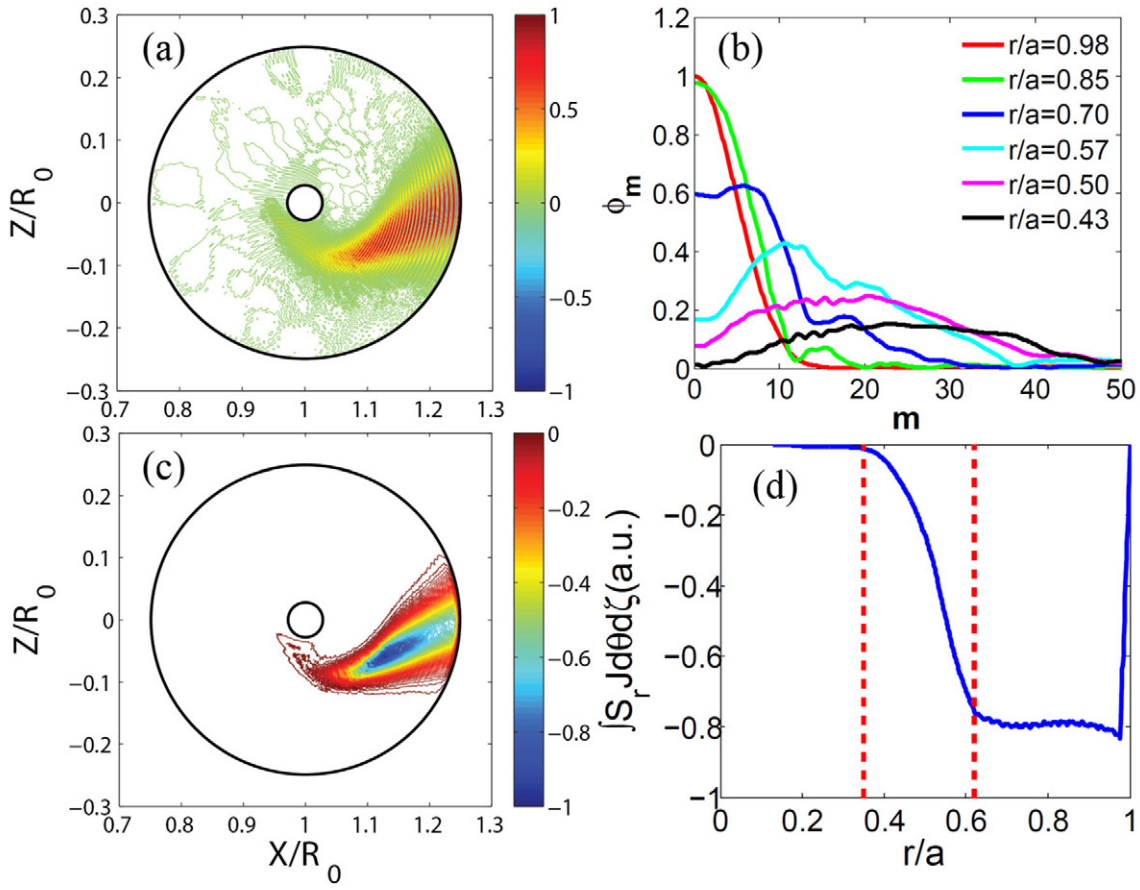

Figure 9. (*a*) A single pass of slow LH wave propagation in the poloidal cross-section. The color scale represents the electrostatic potential ϕ in arbitrary units. Panel (*b*) shows the poloidal spectra of the wave-packets at different flux-surfaces. Panels (*c*) shows the radial component of the energy flux density S_r in the poloidal cross-section, and the color scale represents S_r in arbitrary units. Panel (*d*) shows the radial dependence of the energy flux $S(r) = \int S_r J \mathrm{d}\theta \mathrm{d}\zeta$, and we can see that the absolute value of the energy flux decreases in the region between the red dashed lines, which is due to the wave power deposition in the plasma through electron Landau damping.

wave experiences a downshift due to the increase of $n_{||}$ when propagating toward the tokamak core. In the core region, the parallel phase velocity is still much higher than the electron thermal speed for the $T_{e0} = 2.0\,\mathrm{keV}$ ($\xi_e = \omega/(k_{||}v_{the}) \approx 5.5$ at $r/a = 0.7$) and $T_{e0} = 5.0\,\mathrm{keV}$ ($\xi_e = \omega/(k_{||}v_{the}) \approx 3.4$ at $r/a = 0.7$) cases, while it is closer to the electron thermal speed for the $T_{e0} = 8.0\,\mathrm{keV}$ ($\xi_e = \omega/(k_{||}v_{the}) \approx 2.6$ at $r/a = 0.7$) case to result in significant Landau damping. It is noticed that higher electron temperature can lead to the larger $k_{||}$ upshift. On the other hand, in the edge region, the incident slow LH wave amplitudes are similar for all three cases, since the electron thermal speed is much lower than the wave parallel phase velocities without enough $k_{||}$ upshift. Similarly, we can see that the fast LH wave amplitude of the $T_{e0} = 8.0\,\mathrm{keV}$ case is lower than the $T_{e0} = 2.0\,\mathrm{keV}$ and $T_{e0} = 5.0\,\mathrm{keV}$ cases in figure 8(*e*). The absorption mechanism for the converted fast LH wave is similar to the incident slow LH wave, which is determined by both the $n_{||}$ evolution and the local electron temperature. Furthermore, it can be seen that LH waves can penetrate the mode conversion layer which is calculated by assuming $m = 0$ as shown by blue lines in figures 8(*d*) and (*e*), which is due to the evolution of $n_{||}$ of the LH waves in toroidal geometry. With increasing the electron temperature, the radial positions of the mode conversion layer in the simulations are found to move outwards in figures 8(*d*) and (*e*), and the trajectories of LH wave propagation and mode conversion are also different in figures 8(*a*)–(*c*), because the electron thermal effect can modify the Hermitian part of the dielectric tensor and cause the differences on the LH dispersion relation as shown from WKB and full wave simulations [56].

We now study the linear absorption and poloidal spectrum evolution of the LH wave-packet during a single pass propagation. The plasma is hot with the axis value of electron temperature $T_{e0} = 8.0\,\mathrm{keV}$. The plasma density on the magnetic axis is $n_{i0} = n_{e0} = 5.0 \times 10^{13}\,\mathrm{cm}^{-3}$, which is much lower than the mode conversion cases and guarantees that the accessibility condition can be satisfied. Both the plasma temperature and the density decrease monotonously from the axis to the edge in our simulation, which is the same with the density profile in figure 2(*b*). We launch the LH wave-packet at the outer mid-plane of the tokamak. It should be pointed out that the electron Landau damping is the only dissipation mechanism of the LH wave in our simulation to maintain the steady state. The LH wave propagation in the poloidal plane is shown in figure 9(*a*), and it is seen that the LH wave is gradually damped while propagating toward the core. The poloidal spectra of the wave-packets at different flux surfaces are shown in figure 9(*b*). The central value of the poloidal

spectrum increases and the spectrum broadens when the wave penetrates towards the core, which is due to the poloidal asymmetry of the magnetic field and the wave diffractions. Figure 9(*c*) shows the radial component of the energy flux density $S_r(r,\theta,\zeta) = \mathbf{E}\times\mathbf{H}|_r$ in the poloidal cross-section. The negative value of S_r indicates that the wave energy flows from the tokamak edge to the core. The integral of S_r over flux-surface $S(r) = \int \mathbf{S_r}\cdot\mathbf{dA} = \int S_r J \mathrm{d}\theta\mathrm{d}\zeta$ (J is Jacobian) is shown in figure 9(*d*). The sharp increase of the energy flux near the edge is due to the finite size of the antenna perturbation. From figure 9(*d*), it is seen that the energy flux of LH wave through each flux-surface is almost constant in the region $r/a > 0.62$ without absorption from plasma. However, its absolute value decreases in the region $0.35 < r/a < 0.62$, which is due to electron Landau damping as the poloidal spectrum up-shifts and broadens and the electron temperature increases when the wave propagates from the edge to the core.

In summary, the poloidal spectrum upshift and broadening effects in the LH wave propagation and mode conversion in tokamak are observed for the first time from global particle-in-cell simulations. These effects could enhance the wave damping due to an increase of the parallel refractive index, which could be candidates for explaining the 'spectral gap' problem [4, 7, 8].

5. Conclusions

The phase and group velocities of the slow and fast LH waves measured from electromagnetic GTC simulation agree well with analytic theory. The mode conversion between slow and fast LH waves has been observed in toroidal simulation if the accessibility condition is not satisfied. The difference between the mode conversion layer calculated by assuming poloidal harmonic $m = 0$ and simulation result is due to the evolution of the parallel refractive index $n_{||}$ which is induced by the toroidicity. Furthermore, our particle simulation verifies that moving the launching position from the low field side toward the high field side can help LH wave penetration into the tokamak core, since propagation in the high field side can lead to a larger upshift of $n_{||}$. Finally, the linear absorptions of LH waves in hot plasmas are observed in our simulation for both the mode conversion and single pass cases. The absorption is mainly determined by the $n_{||}$ evolution and the local electron temperature. The linear upshift and broadening effects of $n_{||}$ during the wave-packet propagation in toroidal geometry are verified by the particle simulation, which can be considered as candidates for explaining the 'spectral gap' problem. In the future work, we will focus on nonlinear absorption and parametric decay instability of LH waves in toroidal geometry.

Acknowledgments

This work was supported by China National Magnetic Confinement Fusion Science Program (Grant No. 2013GB111000) and US Department of Energy (DOE) SciDAC GSEP Program. This work used resources of the Oak Ridge Leadership Computing Facility at Oak Ridge National Laboratory (DOE Contract No. DE-AC05-00OR22725) and the National Energy Research Scientific Computing Center (DOE Contract No. DE-AC02-05CH11231). JB acknowledges support from China Scholarship Council (Grant No. 201306010032), and thanks the encouragement from and useful discussions with L. Chen, N.J. Fisch, M. Porkolab, W.W. Lee, F. Zonca, J.C. Wright, Z.X. Lu, N. Xiang, Z.Yu, D.H. Li and GTC team.

References

[1] Fisch N.J. 1978 *Phys. Rev. Lett.* **41** 873
[2] Fisch N.J. 1987 *Rev. Mod. Phys.* **59** 175–234
[3] Reiman A.H. 1983 *Phys. Fluids* **26** 1338
[4] Gormezano C. *et al* 2007 *Nucl. Fusion* **47** S285–336
[5] Bonoli P.T. and Ott E. 1982 *Phys. Fluids* **25** 359
[6] Wright J.C., Bonoli P.T., Schmidt A.E., Phillips C.K., Valeo E.J., Harvey R.W. and Brambilla M.A. 2009 *Phys. Plasmas* **16** 072502
[7] Shiraiwa S., Meneghini O., Parker R., Bonoli P.T., Garrett M., Kaufman M.C., Wright J.C. and Wukitch S. 2010 *Phys. Plasma* **17** 056119
[8] Lu Z.X., Zonca F. and Cardinali A. 2013 *Phys. Plasmas* **20** 032115
[9] Karney C.F.F., Fisch N.J. and Jobes F.C. 1985 *Phys. Rev.* A **32** 2554
[10] Bonoli P.T. and Englade R.C. 1986 *Phys. Fluids* **29** 2937
[11] Pereverzev G.V. 1992 *Nucl. Fusion* **32** 1091
[12] Wallace G.M. *et al* 2010 *Phys. Plasmas* **17** 082508
[13] Porkolab M., Bernabei S., Hooke W.M., Motley R.W. and Nagashima T. 1977 *Phys. Rev. Lett.* **38** 230
[14] Baek S.G. *et al* 2013 *Plasma Phys. Control. Fusion* **55** 052001
[15] Baek S.G. *et al* 2014 *Phys. Plasmas* **21** 012506
[16] Porkolab M. 1974 *Phys. Fluids* **17** 1432
[17] Tripathi V.K., Grebogi C. and Liu C.S. 1977 *Phys. Fluids* **20** 1525
[18] Liu C.S., Tripathi V.K., Chan V.S. and Stefan V. 1984 *Phys. Fluids* **27** 1709
[19] Zhao A.H. and Gao Z. 2013 *Nucl. Fusion* **53** 083015
[20] Lin Y., Wang X.Y., Lin Z. and Chen L. 2005 *Plasma Phys. Control. Fusion* **47** 657
[21] Qi L., Wang X.Y. and Lin Y. 2013 *Phys. Plasmas* **20** 062107
[22] Li D., Xiang N., Lin Y., Wang X.Y., Yang C. and Ma J. 2014 *Plasma Sci. Technol.* **16** 821
[23] Nieter C. and Cary J.R. 2004 *J. Comput. Phys.* **196** 448
[24] Gan C.Y., Xiang N., Ou J. and Yu Z. 2015 *Nucl. Fusion* **55** 063002
[25] Qin H. and Tang W.M. 2004 *Phys. Plasmas* **11** 1052
[26] Yu Z. and Qin H. 2009 *Phys. Plasmas* **16** 032507
[27] Bao J., Lin Z., Kuley A. and Lu Z.X. 2014 *Plasma Phys. Control. Fusion* **56** 095020
[28] Bao J., Lin Z., Kuley A. and Wang Z.X. 2016 arXiv:1602.06554
[29] Kuley A., Wang Z.X., Lin Z. and Wessel F. 2013 *Phys. Plasmas* **20** 102515
[30] Kuley A., Lin Z., Bao J., Wei X.S., Xiao Y., Sun G.Y. and Fisch N.J. 2015 *Phys. Plasmas* **22** 102515
[31] Wei X.S., Xiao Y., Kuley A. and Lin Z. 2015 *Phys. Plasmas* **22** 092502
[32] Lin Z., Hahm T.S., Lee W.W., Tang W.M. and White R.B. 1998 *Science* **281** 1835
[33] Lin Z., Tang W.M. and Lee W.W. 1997 *Phys. Rev. Lett.* **78** 456
[34] Lin Z., Tang W.M. and Lee W.W. 1995 *Phys. Plasmas* **2** 2975

[35] Zhang W.L., Lin Z. and Chen L. 2008 *Phys. Rev. Lett.* **101** 095001
[36] Xiao Y. and Lin Z. 2009 *Phys. Rev. Lett.* **103** 085004
[37] Zhang H.S., Lin Z. and Holod I. 2012 *Phys. Rev. Lett.* **109** 025001
[38] Wang Z.X. *et al* 2013 *Phys. Rev. Lett.* **111** 145003
[39] Deng W., Lin Z. and Holod I. 2012 *Nucl. Fusion* **52** 023005
[40] McClenaghan J., Lin Z., Holod I., Deng W. and Wang Z.X. 2014 *Phys. Plasmas* **21** 122519
[41] Liu D., Zhang W., McClenaghan J., Wang J. and Lin Z. 2014 *Phys. Plasmas* **21** 122520
[42] Xiao Y., Holod I., Wang Z.X., Lin Z. and Zhang T.G. 2015 *Phys. Plasmas* **22** 022516
[43] Bonoli P.T. 2014 *Phys. Plasmas* **21** 061508
[44] Ignat D.W. 1981 *Phys. Fluids* **24** 1110
[45] Stix T.H. 1992 *Waves in Plasmas* (New York: AIP)
[46] Prater R., Moeller C.P., Pinsker R.I., Porkolab M., Meneghini O. and Vdovin V.L. 2014 *Nucl. Fusion* **54** 083024
[47] ITER Physics Basis 1999 *Nucl. Fusion* **39** 12
[48] Bonoli P.T. *et al* 2008 *Phys. Plasmas* **15** 056117
[49] Baek S.G. I 2014 *AIP Conf. Proc.* **1580** 121
[50] Woods A.M., Cairns R.A. and Lashmore-Davies C.N. 1986 *Phys. Fluids* **29** 3719
[51] Jia G.Z. and Gao Z. 2014 *Phys. Plasmas* **21** 122121
[52] Bonoli P.T. 2014 *Bull. Am. Phys. Soc.* **59** 15
[53] Wallace G.M. *et al* 2015 *AIP Conf. Proc.* **1689** 030017
[54] Ochs I.E., Bertelli N. and Fisch N.J. 2015 *Phys. Plasma* **22** 082119
[55] Ochs I.E., Bertelli N. and Fisch N.J. 2015 *Phys. Plasma* **22** 112103
[56] Wright J.C. and Bertelli N. 2014 *Plasma Phys. Control. Fusion* **56** 035006